J. Chem. Soc. Nigeria, Vol. 50, No. 4, pp 835 – 858 [2025] https://dx.doi.org/10.4314/jcsn.v50i4.12

VIRTUAL SCREENING AND MACHINE LEARNING-BASED IDENTIFICATION OF TROPICAL PLANT METABOLITES WITH MULTIPLE *Mycobacterium ulcerans* PROTEIN TARGETING POTENTIAL IN BURULI ULCER MANAGEMENT

C. E. Duru[1,2*], C. N. Nwofor[3], U. J. M. Ikezu[1], C. E. Enyoh[4]

[1]Department of Chemistry, Imo State University, Owerri, Nigeria
[2]Theoretical and Computational Chemistry Research Group, Department of Chemistry, Imo State University, Owerri, Nigeria
[3]Department of Microbiology, Imo State University, Owerri, Nigeria
[4]Graduate School of Science and Engineering, Saitama University, Saitama, Japan
*Corresponding author – chidiedbertduru@gmail.com

ABSTRACT

Buruli ulcer, a debilitating skin disease caused by *Mycobacterium ulcerans*, remains a neglected tropical disease with limited and often toxic treatment options. This study investigates the therapeutic potential of tropical medicinal plants using integrative computational strategies to identify bioactive compounds targeting key *M. ulcerans* proteins. Nine African plant species were analyzed via gas chromatography-mass spectrometry (GC-MS), yielding 217 phytochemicals. These were screened against four essential *M. ulcerans* enzymes - Cytochrome P450, Phosphopantetheinyl transferase, Dihydrofolate reductase, and Lysyl-tRNA synthetase using validated molecular docking protocols. ADME profiling evaluated pharmacokinetics and druglikeness, while Principal Component Analysis (PCA) explored the influence of physicochemical properties on target affinity. Machine learning-based AutoQSAR modeling was used to predict minimum inhibitory concentrations (MICs). Hit compounds such as 12-(acetyloxy)-17-(1-methyl-4-oxo-5-phenylpentyl)gonan-3-yl acetate (AMPA) from *Phyllanthus amarus* and ergosta-5,24-dienol from *Ageratum conyzoides* showed strong binding affinities, outperforming native ligands. AMPA demonstrated the most potent predicted MIC (1.20 µg/mL), comparable to standard antibiotics and superior to previously reported phytochemicals. ADME and PCA analyses highlighted lipophilicity and hydrogen bonding as key factors in target engagement. This study validates the ethnopharmacological relevance of tropical plants and illustrates how AI-driven screening can accelerate the discovery of plant-derived therapies. The findings offer a foundation for in vitro validation and rational development of accessible, low-toxicity treatments for Buruli ulcer.

Keywords: Buruli ulcer; *Mycobacterium ulcerans*; Molecular docking; Principal Component Analysis; AutoQSAR

INTRODUCTION

Buruli ulcer is a chronic, necrotizing skin disease caused by *Mycobacterium ulcerans*, a slow-growing environmental mycobacterium that produces the immunosuppressive and cytotoxic macrolide toxin, mycolactone. The disease is characterized by progressive and painless necrosis of skin, subcutaneous fat, and in severe cases, underlying bone. As one of the 17 neglected tropical diseases (NTDs) prioritized by the World Health Organization (WHO), Buruli ulcer poses a significant public health challenge, particularly in low- and middle-income countries

ISSN 0795 - 22066

where diagnostic, therapeutic, and preventive resources are often limited. First identified in Uganda in the mid-20th century, the disease was named after Buruli County, where outbreaks were notably documented in the 1960s [1]. WHO formally recognized Buruli ulcer as a re-emerging public health concern at the Yamoussoukro Conference in 1998, due to its increasing prevalence and devastating impact on affected communities [2].

As of recent global epidemiological reports, Buruli ulcer has been identified in over 33 countries across Africa, South America, Asia, and the Western Pacific, with the heaviest burden concentrated in sub-Saharan Africa. Countries such as Ghana, Côte d'Ivoire, Benin, Nigeria, Cameroon, and Gabon consistently report high incidence rates [3]. The disease disproportionately affects children under the age of 15 and individuals residing near slow-flowing water bodies, although the exact environmental reservoir and transmission mechanisms of *M. ulcerans* remain poorly understood. The lack of definitive knowledge about transmission continues to hinder the development of targeted public health interventions [4]. Clinically, Buruli ulcer progresses through three distinct stages. The initial pre-ulcerative stage presents as a painless nodule, plaque, or edema, which may be mistaken for other dermatological conditions. This stage often progresses rapidly to the ulcerative phase, marked by extensive skin breakdown, undermined edges, and exposure of subcutaneous tissue. In the absence of timely and effective treatment, Buruli ulcer can finally progress to severe and debilitating complications, including the development of contractures and joint deformities. In some cases, the destruction extends to deeper tissues, including tendons and bones, necessitating surgical intervention or amputation [5].

The pathogenicity of *M. ulcerans* is largely attributed to its arsenal of specialized proteins that coordinate immune evasion, cellular invasion, toxin production, and structural integrity. Among these, cytochrome P450 enzymes are critical in the biosynthetic pathway of mycolactone, enabling its assembly and function [6]. Phosphopantetheinyl transferase activates mycolactone precursors and facilitates their export, allowing for interaction with host cells [7]. Dihydrofolate reductase supports folate metabolism, which is essential for nucleic acid synthesis and microbial replication [8]. Additionally, lysyl-tRNA synthetase is integral to protein biosynthesis, including the synthesis of virulence factors [9]. Other structural and functional proteins such as Antigen 85 complex (Ag85), involved in mycobacterial cell wall synthesis [10], ESAT-6, a secreted protein that disrupts host cell membranes and impairs immune signaling [11], and mycobacterial membrane protein large (MmpL), which transports lipids and molecules across the cell membrane [12], further contribute to disease progression and host damage. Together, these virulence factors enable *M. ulcerans* to establish

ISSN 0795 - 22066

chronic infection, evade host immune defenses, and cause extensive tissue destruction.

Current WHO guidelines recommend an 8-week antibiotic regimen comprising oral rifampicin (10 mg/kg/day) and intramuscular streptomycin (15 mg/kg/day for the first 4 weeks) as the primary treatment for Buruli ulcer. Rifampicin acts by inhibiting the DNA-dependent RNA polymerase of *M. ulcerans*, thereby halting bacterial transcription and growth [13]. Streptomycin binds to the 30S ribosomal subunit, disrupting protein synthesis and inducing bacterial cell death [14]. While this combination therapy has proven effective in bacterial clearance and lesion resolution in many cases, it presents significant limitations. Adverse effects such as hepatotoxicity (rifampicin) and ototoxicity or nephrotoxicity (streptomycin) are common [15]. Additionally, streptomycin's injectable form complicates outpatient treatment, reduces patient adherence, and increases healthcare costs. The prolonged treatment duration also elevates the risk of drug resistance, treatment discontinuation, and recurrence [16]. Furthermore, antibiotic therapy is less effective against late-stage lesions, where extensive necrosis often necessitates surgical excision to promote healing and prevent disability. Given these limitations, alternative and adjunctive therapeutic strategies are urgently needed, particularly in resource-limited settings where access to antibiotics and surgical services is constrained. One promising avenue involves the use of herbal medicine, which has a long-standing history in the management of skin diseases and wound healing in endemic regions. Traditional plant-based therapies are widely used for Buruli ulcer in rural Africa, and some have shown antimicrobial and anti-inflammatory properties in preclinical studies [17]. Herbal remedies are typically more accessible, culturally accepted, and cost-effective, making them a feasible alternative to conventional treatment in underserved populations. Moreover, the polypharmacological nature of plant extracts-containing multiple bioactive compounds, may offer synergistic effects that target bacterial viability, toxin activity, and host immune modulation simultaneously [18]. Nevertheless, the therapeutic potential of plant-derived compounds remains underexplored at the molecular level. Crude extracts, while rich in bioactive constituents, present challenges due to their compositional complexity, potential for toxicity, and variability in pharmacokinetics. Therefore, the identification and characterization of individual active metabolites are essential for developing standardized and effective phytotherapeutics. Advances in computational drug discovery, particularly virtual screening, molecular docking, and machine learning, have enabled the rapid identification of lead compounds from complex chemical libraries, significantly accelerating early-stage drug development.

In this study, we employed an integrative computational approach to identify plant-derived secondary metabolites with potential inhibitory

ISSN 0795 - 22066

activity against key *M. ulcerans* virulence proteins. Using molecular docking, we screened compounds for binding affinity and interaction with selected protein targets implicated in mycolactone biosynthesis, immune modulation, and bacterial survival. ADME (absorption, distribution, metabolism, and excretion) profiling was then conducted to evaluate druglikeness and pharmacokinetic properties of the most promising compounds. To further understand the relationship between molecular properties and biological activity, Principal Component Analysis (PCA) and Quantitative Structure–Activity Relationship (QSAR) modeling were applied. Finally, we estimated the minimum inhibitory concentrations (MICs) of hit compounds and compared them with standard antibiotics at a representative *M. ulcerans* target. This comprehensive in silico analysis aims to uncover novel phytochemicals with anti-mycobacterial potential and lay the groundwork for future experimental validation and therapeutic development against Buruli ulcer.

MATERIALS AND METHODS

Plant collection and extraction

The in vitro antimicrobial properties of various tropical plant extracts against *Mycobacterium ulcerans* have been previously documented [19]. In the present study, nine medicinal plants of tropical African origin were selected based on their reported ethnopharmacological relevance. These included *Erythrophleum suaveolens* (stem bark), *Newbouldia laevis* (stem bark), *Bryophylum pinnatum* (leaf), *Ageratum conyzoides* (leaf), *Phyllanthus amarus* (leaf), *Psidium guajava* (leaf), *Allium sativum* (bulb), *Syzygium aromaticum* (flower bud), and *Zanthoxylum zanthoxyloides* (root). Plant materials were freshly collected from local sources and taxonomically authenticated by a qualified botanist in the Department of Plant Science and Biotechnology, Imo State University, Owerri, Nigeria. Voucher specimens were prepared and deposited in the departmental herbarium for reference. Each plant part was washed thoroughly with deionized water to eliminate surface contaminants and air-dried under aseptic conditions on sterile cotton cloths at room temperature to remove residual moisture. Dried materials were subsequently pulverized to a fine powder using a sterile porcelain mortar and pestle. For extraction, 5 g of each powdered sample was subjected to cold maceration in 50 mL of 70 % ethanol for 24 hours at ambient temperature, with intermittent agitation. The macerated mixtures were filtered through Whatman No. 1 filter paper, and the resulting filtrates were concentrated under reduced pressure using a rotary evaporator to obtain the crude ethanolic extracts. These extracts were then stored at 4 °C until further analyses.

GC-MS analysis of plant extract

The phytochemical profiling of the plant extracts was performed using Gas Chromatography–Mass Spectrometry (GC–MS) analysis, following the method described by [20]. The analysis was

ISSN 0795 - 22066

conducted using an Agilent Technologies GC–MS system (Model: 7890 GC coupled with 5977B Mass Selective Detector, USA). Each extract was subjected to full-scan mode within a mass-to-charge ratio (m/z) range of 40–500. The resulting mass spectra were interpreted and matched against reference spectra from the National Institute of Standards and Technology (NIST) Mass Spectral Library using the integrated library search software. Phytochemical constituents were identified based on spectral similarity and retention indices.

Docking validation

The molecular docking protocol was rigorously validated to ensure its accuracy and reliability in reproducing the co-crystallized ligand's binding pose and molecular interactions within the protein structure. For each protein target, the corresponding native ligand was retrieved from the PubChem database and subjected to energy minimization using PyRx's virtual screening tool. The minimized ligand was then re-docked into the active site of its respective protein structure using AutoDock Vina, integrated within the PyRx platform. To evaluate the fidelity of the docking procedure, the resulting docked ligand–protein complex was superimposed onto the original X-ray crystallographic structure (obtained from the Protein Data Bank, PDB) containing the co-crystallized ligand. The resulting docked complex was superimposed onto the X-ray-resolved crystal structure of the protein (obtained from PDB) bearing the co-crystallized ligand, yielding a root mean square deviation (RMSD) value calculated using PyMOL. The RMSD values obtained were within the generally accepted threshold of 0–2 Å [21], thereby confirming the robustness and reliability of the docking protocol for subsequent virtual screening and interaction prediction between the target proteins and selected small-molecule inhibitors.

Molecular docking analysis

A total of 217 phytochemicals identified through GC–MS analysis of the crude plant extracts were selected for in silico analysis. The three-dimensional (3D) structures of these compounds were retrieved from the PubChem database in Structure Data File (SDF) format. Molecular geometry optimization was subsequently performed using Open Babel integrated within the Python Prescription platform (version 0.8), applying the Merck Molecular Force Field 94 (MMFF94) algorithm to generate the energetically most favorable conformations. The 3D crystal structures of four key *Mycobacterium ulcerans* protein targets were obtained from the Protein Data Bank (PDB) for molecular docking studies. These targets included: Cytochrome P450 enzyme (PDB ID: 7SH5), Phosphopantetheinyl transferase (PDB ID: 4QJL), Dihydrofolate reductase (PDB ID: 6UWW), and Lysyl-tRNA synthetase (PDB ID: 6AQG). These proteins were selected based on their established roles in *M. ulcerans*

ISSN 0795 - 22066

pathogenicity and viability, as illustrated in Figure 1.

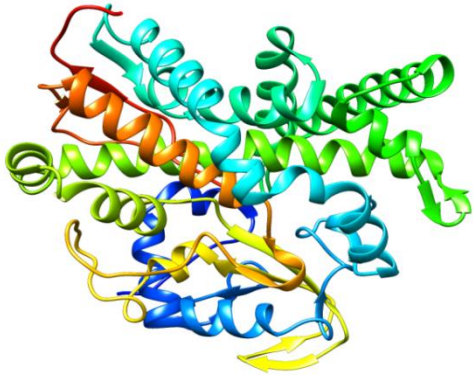

Cytochrome P450 enzyme from *M. ulcerans* (PDB ID: 7SH5)

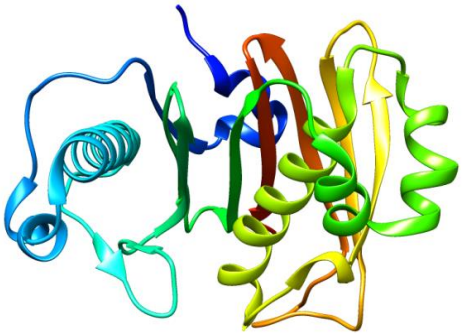

Phosphopantetheinyl transferase (PDB ID: 4QJL)

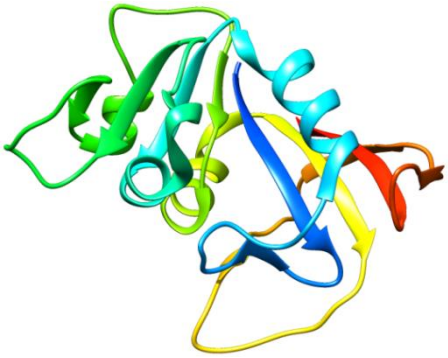

Dihydrofolate reductase (PDB ID: 6UWW)

Lysyl-tRNA synthetase (PDB ID: 6AQG)

Figure 1: *Mycobacterium ulcerans* proteins used in this study

Protein structures were prepared for molecular docking by removing all non-essential residues, co-crystallized ligands, and solvent molecules. Energy minimization of the cleaned protein structures was performed using Cresset Flare® software (version 4.0), applying the General AMBER Force Field (GAFF). The minimization protocol was executed with a gradient convergence criterion of 0.200 kcal/mol/Å and a maximum of 2000 iterations to ensure structural stability and reduce steric clashes. Docking simulations were conducted using a flexible docking protocol as described by [22], employing the Python Prescription 0.8 platform, which integrates the AutoDock Vina engine. Prior to docking, the ligand molecules (in SDF format) obtained from PubChem were energy-minimized using the PyRx virtual screening tool. This minimization was performed using the Universal

ISSN 0795 - 22066

Force Field (UFF) with a step count of 300. The optimized ligand structures were then converted to AutoDock-compatible format (pdbqt) for further analysis.

Protein structures were similarly prepared by adding all polar hydrogen atoms, assigning Gasteiger partial atomic charges, and converting the refined structures into the pdbqt format required for docking in AutoDock Vina. Binding sites on each target protein were defined using grid boxes centered on the active site, with dimensions specified in Table 1. Following the docking simulations, the resulting ligand–protein interaction complexes were analyzed to identify key binding residues. Visualization and interaction profiling were carried out using BIOVIA Discovery Studio Visualizer (version 20.1), enabling detailed analysis of hydrogen bonds, hydrophobic interactions, and other non-covalent binding features between the lead phytochemicals and the active site residues of the protein targets [23-24].

Table 1: Grid box sizes of the binding sites at the protein targets

Protein ID	Center	Size
7SH5	x = -12.569; y = -13.057; z = 6.691	x = 28.953; y = 32.241; z = 30.614
4QJL	x = 12.254; y = 11.614; z = 21.311	x = 29.806; y = 28.127; z = 25.000
6UWW	x = -1.430; y = -1.660; z = 14.259	x = 24.839; y = 23.636; z = 22.821
6AQG	x = 15.037; y = 4.671; z = 5.212	x = 21.340; y = 23.309; z = 25.202

Druglikeness evaluation based on ADME parameters

The drug-likeness of the identified hit compounds was assessed using ADMETlab 3.0, which evaluates physicochemical and pharmacokinetic parameters. Compliance with Lipinski's Rule of Five was examined, including molecular weight, lipophilicity (log P), hydrogen bond acceptors, and donors. Additionally, topological polar surface area (TPSA), number of rotatable bonds, and molecular flexibility were analyzed to predict the compounds' potential success as drug candidates.

Unsupervised machine learning- Principal Component Analysis (PCA)

This study employed Principal Component Analysis (PCA), a dimensionality reduction technique and unsupervised machine learning approach, to identify patterns and relationships between the ligands' ADME physicochemical properties and their binding affinities to different proteins. The analysis considered key ADME parameters, including lipophilicity (Log P), molecular weight (MW), hydrogen bond donors (HBD), hydrogen bond acceptors (HBA), topological polar surface area (TPSA), number of atoms (nA), rotatable bonds (nRB), and rings (nRing). Following standardization of the dataset

ISSN 0795 - 22066

to ensure equal contribution of variables, PCA was performed using OriginLab Pro, retaining principal components with eigenvalues greater than 1. The results were interpreted using loading plots, score plots, and biplots, which revealed the contribution of ADME parameters to principal components, clustering of ligands based on ADME properties, and correlations between physicochemical properties and protein binding affinities, providing insights into the influence of ADME descriptors on ligand-target interactions.

QSAR modeling for antibacterial activity of hit compounds against M. ulcerans

A Quantitative Structure-Activity Relationship (QSAR) model was developed to predict the Minimum Inhibitory Concentration (MIC) of the hit compounds against *Mycobacterium ulcerans*. A dataset of 10 antibiotic inhibitors was retrieved from the CHEMBL database and converted to SDF format using Data Warrior software. The Auto QSAR module in Schrödinger was used to construct multiple models, and the best-performing model (kpls_dendritic_37) was selected based on its rank and predictive capability. The model was trained using molecular descriptors, including topological indices, physicochemical properties, and electronic features, and evaluated using statistical metrics. The model's predictive capability was demonstrated by its ability to estimate pMIC values for hit compounds and standard antibiotics, enabling the prediction of their MIC values and potential antibacterial activity against *M. ulcerans*.

Table 2: Train and test sets for the QSAR model

ID	Set	Name	Y (Observed)	Y (Predicted)	Error
1	Test	CHEMBL1384	5.3010	5.1115	-0.1896
2	Train	CHEMBL32	7.7959	7.4087	-0.3872
3	Train	CHEMBL372795	6.6021	6.1055	-0.4965
4	Train	CHEMBL374478	7.7959	8.2620	0.4661
5	Train	CHEMBL1741	6.6021	6.3157	-0.2863
6	Train	CHEMBL1440	5.6021	5.6345	0.0324
7	Test	CHEMBL126	6.0000	5.7179	-0.2821
8	Train	CHEMBL64	4.3979	4.7872	0.3893
9	Train	CHEMBL532	6.0000	6.3046	0.3046
10	Train	CHEMBL1276484	4.9031	4.8807	-0.0224

ISSN 0795 - 22066

RESULTS AND DISCUSSION

Molecular docking studies

Gas chromatography–mass spectrometry (GC–MS) was employed to comprehensively profile the phytochemical constituents of nine medicinal plants of tropical African origin, namely *Erythrophleum suaveolens* (stem bark), *Newbouldia laevis* (stem bark), *Bryophyllum pinnatum* (leaf), *Ageratum conyzoides* (leaf), *Phyllanthus amarus* (leaf), *Psidium guajava* (leaf), *Allium sativum* (bulb), *Syzygium aromaticum* (flower bud), and *Zanthoxylum zanthoxyloides* (root). The GC–MS analysis identified a total of 217 unique phytochemical compounds across the various plant parts. These metabolites were subsequently subjected to structure-based virtual screening via molecular docking against four validated *Mycobacterium ulcerans* protein targets: Cytochrome P450 (PDB ID: 7SH5), Phosphopantetheinyl transferase (PDB ID: 4QJL), Dihydrofolate reductase (PDB ID: 6UWW), and Lysyl-tRNA synthetase (PDB ID: 6AQG).

Molecular docking was employed as a predictive computational approach to evaluate the binding affinity and orientation of the identified phytochemicals within the active sites of the protein targets. This method simulates ligand–receptor interactions by generating multiple binding poses and ranking them using scoring functions that approximate binding free energy, thereby enabling the identification of potential hit compounds. Docking studies serve as an integral part of structure-based drug discovery, facilitating the rapid assessment of large compound libraries against target proteins.

To ensure the reliability and predictive accuracy of the docking simulations, the protocol was validated through self-docking (re-docking) experiments. In these validations, the co-crystallized ligands of each target protein were extracted, energy-minimized, and re-docked into their native binding pockets. The resulting ligand poses were then compared to their experimentally determined conformations using root mean square deviation (RMSD) analysis. The observed RMSD values were 1.476 Å (7SH5), 1.919 Å (4QJL), 1.021 Å (6UWW), and 1.831 Å (6AQG), all of which fall within the generally accepted threshold of < 2.0 Å for successful docking protocol validation. These results confirm the robustness and fidelity of the employed docking methodology in accurately predicting ligand–protein interactions for the investigated phytochemicals.

Despite significant advancements in modern medicine, the therapeutic management of mycobacterial infections, including tuberculosis, leprosy, and Buruli ulcer remains suboptimal. The persistent challenge of drug resistance, coupled with the limited efficacy of existing antimycobacterial agents, underscores the urgent need for the discovery and development of novel therapeutic compounds with improved pharmacological profiles. Natural products, particularly those derived from medicinal plants, have historically served as a valuable source of

ISSN 0795 - 22066

bioactive compounds with antimicrobial potential. Several in vitro studies have demonstrated the inhibitory effects of plant extracts against *Mycobacterium* spp., highlighting their potential utility as leads for antimycobacterial drug development. Notably, *Phyllanthus amarus* has been extensively evaluated for its antimycobacterial activity. A study investigated the in vitro effects of aqueous and ethanolic extracts of *P. amarus* on seven clinical isolates of *Mycobacterium ulcerans* obtained from various regions in Côte d'Ivoire [25]. Both extracts exhibited consistent and effective inhibitory activity across all tested strains, with comparable minimum inhibitory concentrations (MICs), indicating broad-spectrum activity against *M. ulcerans*. Further evidence of the antimycobacterial efficacy of *P. amarus* was provided by [26], who evaluated the activity of its aqueous extract against two strains of *Mycobacterium tuberculosis* (H37Rv and RF94) and one strain of *M. ulcerans*. The MIC values were determined to be 16 mg/mL for the RF94 strain and 64 mg/mL for both H37Rv and *M. ulcerans*, suggesting selective activity that warrants further investigation.

In addition to *P. amarus*, other plant species have shown promise as sources of antimycobacterial agents. The in vivo antimycobacterial activity of the crude hydroethanolic extract from the aerial parts of *Holarrhena floribunda* against *M. ulcerans* has been reported to have significant activity [27]. Phytochemical analysis of the extract led to the identification of four steroidal alkaloids (Figure 2) as the principal bioactive constituents. Among them, 3-methylamino-pregn-5,16-dien-20-ol was identified as the predominant compound, exhibiting superior antimycobacterial activity compared to the other alkaloids isolated. These findings collectively support the potential of tropical medicinal plants as rich reservoirs of bioactive secondary metabolites with inhibitory activity against pathogenic mycobacteria and provide a strong rationale for further exploration through integrative approaches such as virtual screening and structure-based drug design.

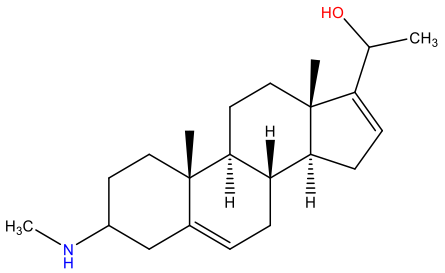

3-methylamino pregn-5,16-dien-20-ol

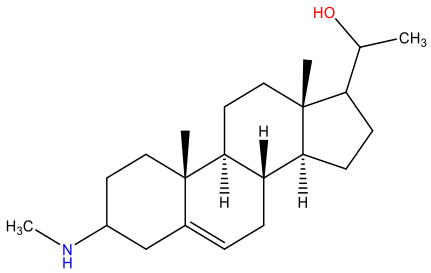

3-methylamino pregn-5-en-20-ol

ISSN 0795 - 22066

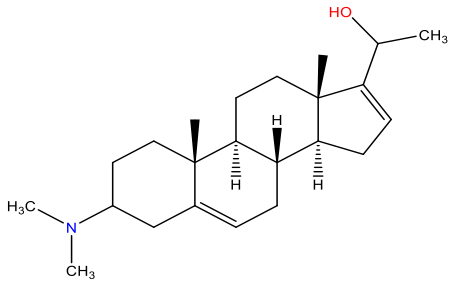

3-dimethylamino pregn-5,16-dien-20-ol

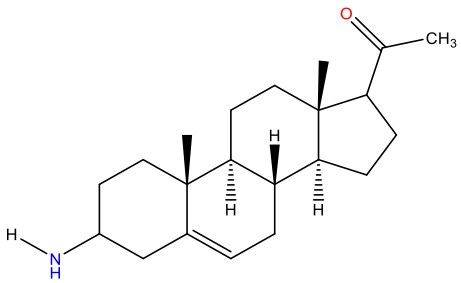

3-amino pregn-5-en-20-one

Figure 2: Steroidal alkaloids reported to have activity against *M. ulcerans*

The binding energy of the major hit compounds at the four protein targets and their plant sources in this study are summarized in Table 3.

The molecular docking analysis identified several phytochemical compounds with high binding affinities toward the *M. ulcerans* protein targets. Notable hit compounds included ergost-7-en-3-ol and ergosta-5,24-dienol from *A. conyzoides*; 12-(acetyloxy)-17-(1-methyl-4-oxo-5-phenylpentyl)gonan-3-yl acetate (AMPA) from *P. amarus*; and A-neooleana-3(5),12-diene, germanicol 3-acetate, and cholest-5-en-3-ol (3β) from *Z. zanthoxyloides* (Figure 3). These compounds demonstrated target-specific binding affinities, with several outperforming the respective native ligands in the docking simulations.

Table 3: Binding energy of hit compounds from different plants at the protein targets

Ligands	Plant Source	PubChem CID	Binding Energy (kcal/mol)			
			7SH5	*4QJL*	*6UWW*	*6AQG*
Ergost-7-en-3-ol	*A. conyzoides*	21116218	-9.5	-8.5	**-9.9***	-7.6
AMPA	*P. amarus*	540444	**-10.5***	-8.2	**-10.2***	**-10.1***
A-neooleana-3(5),12-diene	*Z. zanthoxyloides*	632542	**-10.8***	-8.5	-8.1	-8.1
Germanicol 3-acetate	*Z. zanthoxyloides*	92156	-9.9	-8.2	-7.0	-8.9
Cholest-5-en-3-ol (3.beta.)-	*Z. zanthoxyloides*	111262	-9.5	**-8.6***	-8.9	-9.2
Ergosta-5,24-dienol	*A. conyzoides*	193567	-9.4	**-8.9***	-9.0	**-9.9***
Native ligand (Control)			**-9.7**	**-8.6**	**-8.5**	**-9.2**

ISSN 0795 - 22066

At the cytochrome P450 target, A-neooleana-3(5),12-diene and AMPA exhibited the highest binding energies of −10.8 kcal/mol and −10.5 kcal/mol, respectively, both surpassing the native ligand's binding energy (−9.7 kcal/mol). Germanicol 3-acetate also showed notable interaction at this site, with a binding energy of −9.9 kcal/mol. Evaluation at the phosphopantetheinyl transferase target revealed ergosta-5,24-dienol as the most potent binder (−8.9 kcal/mol), followed by cholest-5-en-3-ol (3β) with a binding energy of −8.6 kcal/mol, comparable to that of the native ligand. Other hit compounds at this site showed slightly lower but still favorable binding energies, ranging between −8.2 and −8.5 kcal/mol. At the dihydrofolate reductase target, AMPA (−10.2 kcal/mol) and ergost-7-en-3-ol (−9.9 kcal/mol) emerged as top binders, both exhibiting stronger affinities than the native ligand (−8.5 kcal/mol). Ergosta-5,24-dienol and cholest-5-en-3-ol (3β) also displayed relatively strong affinities, with binding energies of −9.0 kcal/mol and −8.9 kcal/mol, respectively. At the lysyl-tRNA synthetase target, AMPA (−10.1 kcal/mol) and ergosta-5,24-dienol (−9.9 kcal/mol) again showed the strongest interactions, outperforming the native ligand (−9.2 kcal/mol). Cholest-5-en-3-ol (3β) matched the native ligand with a binding energy of −9.2 kcal/mol, while A-neooleana-3(5),12-diene and germanicol 3-acetate exhibited moderately lower affinities. Overall, AMPA consistently demonstrated high binding affinities across multiple targets (7SH5, 6UWW, and 6AQG), suggesting its broad inhibitory potential. Ergosta-5,24-dienol also exhibited notable activity at 4QJL and 6AQG, while A-neooleana-3(5),12-diene showed strong target engagement at 7SH5. These compounds outperformed or matched the binding affinities of native ligands at their respective sites, highlighting their potential as promising scaffolds for the development of novel antimycobacterial agents.

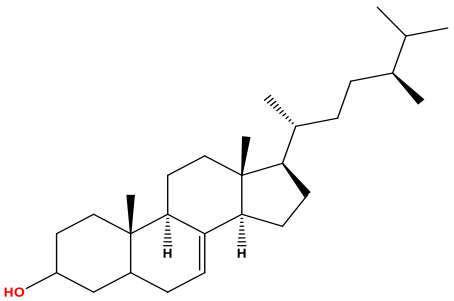

Ergost-7-en-3-ol

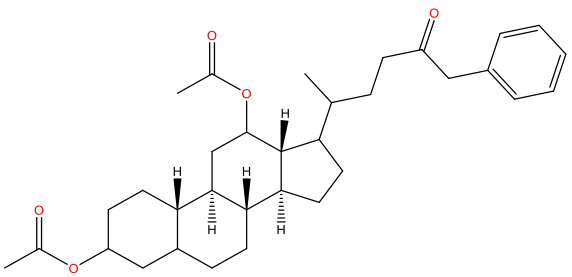

12-(acetyloxy)-17-(1-methyl-4-oxo-5-phenylpentyl)gonan-3-yl acetate (AMPA)

ISSN 0795 - 22066

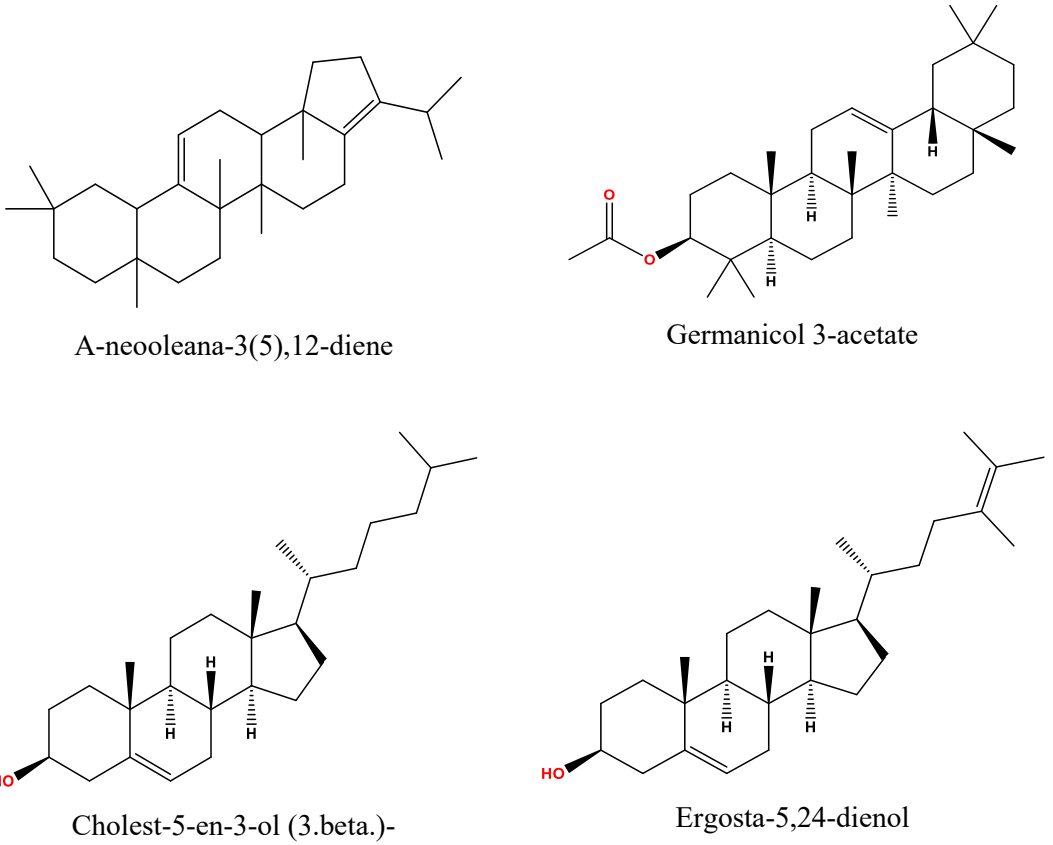

Figure 3: Structure of hit compounds from the studied tropical plant parts

Interestingly, many of the identified hit compounds are steroids or steroidal derivatives, including ergost-7-en-3-ol, ergosta-5,24-dienol, cholest-5-en-3-ol (3β), and AMPA. These molecules share structural similarities with steroidal alkaloids previously reported to exhibit antimycobacterial activity against *M. ulcerans* [27]. The convergence of these findings supports the hypothesis that the steroidal scaffold represents a viable chemotype for designing new inhibitors targeting *M. ulcerans*, thereby offering a promising avenue for the development of effective therapeutic agents against Buruli ulcer.

Druglikeness metrics of hit compounds from ADME analyses

The physicochemical properties of a molecule, encompassing molecular weight (MW), number of atoms (nA), number of rings (nRing), hydrogen bond donors (HBD), hydrogen bond acceptors (HBA), octanol-water partition coefficient (logP), number of rotatable bonds (nRB), and topological polar surface area (TPSA), are pivotal determinants of its druglikeness. These properties exert a profound influence on the molecule's ADME profiles, thereby impacting its overall pharmacokinetic and pharmacodynamic behavior. A comprehensive analysis of these properties enable researchers to predict a compound's potential as a viable drug candidate, identify potential liabilities, and pinpoint areas for

ISSN 0795 - 22066

optimization to enhance its druglikeness. The druglikeness profiles of the identified hit compounds were compared to those of Rifampicin and Streptomycin, two established antibiotics that are integral to the standard treatment regimen for *M. ulcerans* infections, with the comparative analysis summarized in Table 4.

Table 4: Druglikeness metrics of hit compounds from ADME evaluation

Compounds	MW	nA	nRing	HBD	HBA	log P	nRB	TPSA	Carcinogenicity
Ergost-7-en-3-ol	400.37	75	4	1	1	7.30	5	20.23	0.90
AMPA	522.33	86	5	0	5	5.35	10	69.67	0.19
A-neooleana-3(5),12-diene	408.38	80	5	0	0	9.05	1	0.00	0.44
Germanicol 3-acetate	468.40	59	5	0	2	4.97	2	26.30	0.85
Cholest-5-en-3-ol (3.beta.)-	448.31	74	4	0	2	8.64	7	26.30	0.91
Ergosta-5,24-dienol	398.35	75	4	1	1	7.69	4	20.23	0.84
Rifampicin	822.41	117	6	6	16	1.49	5	220.15	0.98
Streptomycin	581.27	79	3	16	19	-1.90	9	336.43	0.05

MW = Molecular weight; nA = Number of Atoms; nRing = Number of Rings; HBD = Hydrogen Bond Donors; HBA = Hydrogen Bond Acceptors; logP = Octanol-Water Partition Coefficient; nRB = Number of Rotatable Bonds; TPSA = Topological Polar Surface Area

A comparative analysis of the physicochemical properties of the identified hit compounds and standard antimycobacterial agents (Rifampicin and Streptomycin) was performed, with results visualized via radial plots (Figure 4). The MW of the phytochemical hits ranged from 398.35 Da for ergosta-5,24-dienol to 522.33 Da for AMPA. In contrast, Rifampicin and Streptomycin exhibited significantly higher molecular weights of 822.41 Da and 581.27 Da, respectively. Given that lower molecular weight is generally associated with improved membrane permeability and oral bioavailability, the phytochemicals, particularly ergosta-5,24-dienol, may offer pharmacokinetic advantages. The log P of the compounds, a key determinant of membrane permeability and drug absorption, also varied markedly. The hit compounds exhibited high lipophilicity, with log P values ranging from 4.97 (germanicol 3-acetate) to 9.05 (A-neooleana-3(5),12-diene), in contrast to Rifampicin (log P = 1.49) and Streptomycin (logP = −1.90), which are considerably more hydrophilic. While moderate lipophilicity is generally favorable for membrane

ISSN 0795 - 22066

diffusion, excessively high log P values may increase the likelihood of off-target toxicity and reduced aqueous solubility, warranting further optimization. Hydrogen bond donor and acceptor counts which are critical factors influencing solubility and permeability also revealed notable differences. Ergost-7-en-3-ol and ergosta-5,24-dienol both possessed 1 HBD and 1 HBA, whereas AMPA had 0 HBD and 5 HBA. In comparison, Rifampicin and Streptomycin had significantly higher polar surface profiles, with Rifampicin contributing 6 HBD and 16 HBA, and Streptomycin contributing 16 HBD and 19 HBA. Excessive hydrogen bonding often correlates with poor membrane permeability, particularly across biological barriers such as the gastrointestinal epithelium. Topological polar surface area, a predictor of drug transport properties such as absorption and blood–brain barrier permeability, ranged from 0.00 Å² for A-neooleana-3(5),12-diene to 69.67 Å² for AMPA among the hit compounds. Rifampicin and Streptomycin had markedly higher TPSA values of 220.15 Å² and 336.43 Å², respectively, substantially exceeding the threshold (typically < 140 Å²) considered favorable for oral bioavailability. These data suggest that several of the phytochemical hits, particularly ergost-7-en-3-ol, ergosta-5,24-dienol, and A-neooleana-3(5),12-diene, possess physicochemical properties that are more compatible with favorable ADME profiles than the current standard drugs.

Collectively, this comparative analysis underscores the potential of the hit phytochemicals as promising leads for further optimization. Their lower molecular weight, moderate hydrogen bonding capacity, and reduced TPSA suggest improved membrane permeability and oral bioavailability, making them attractive candidates for the development of novel therapeutics targeting *M. ulcerans* infections.

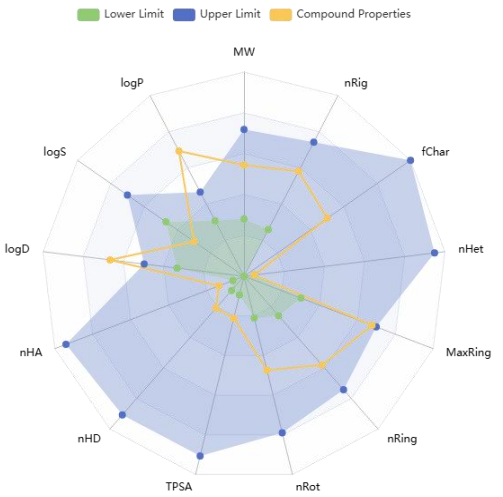

Ergost-7-en-3-ol

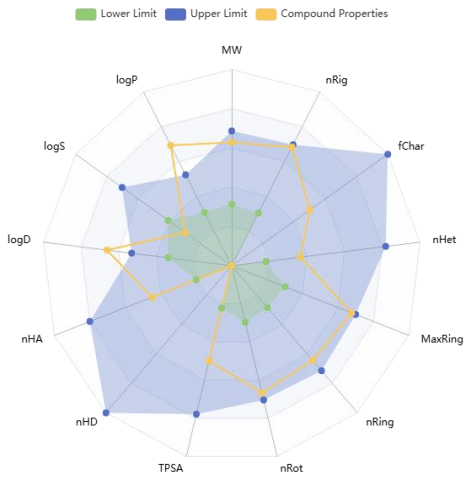

AMPA

ISSN 0795 - 22066

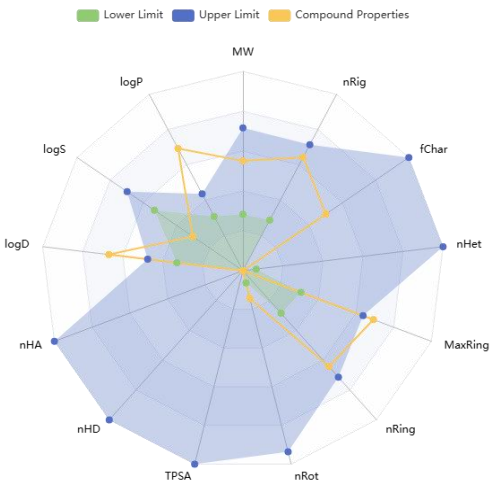

A-neooleana-3(5),12-diene

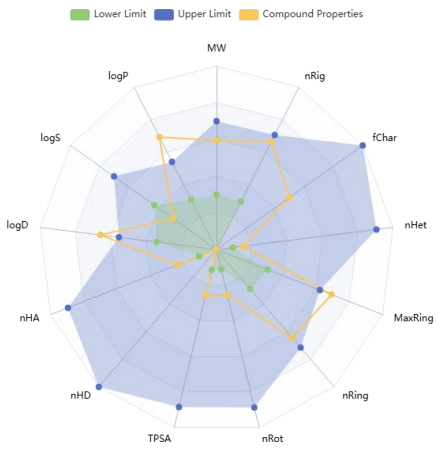

Germanicol 3-acetate

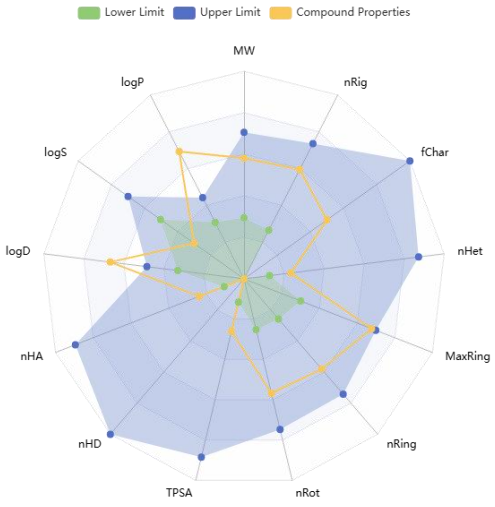

Cholest-5-en-3-ol (3.beta.)-

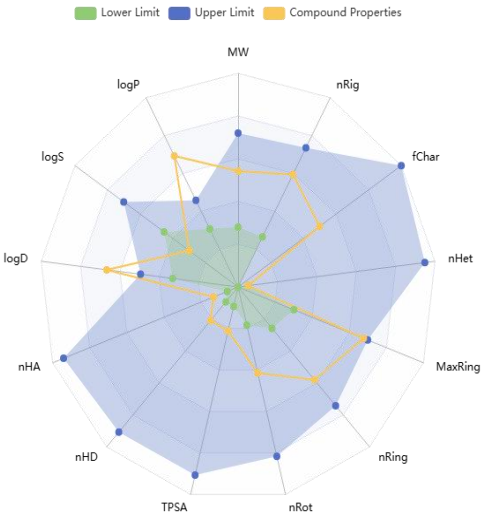

Ergosta-5,24-dienol

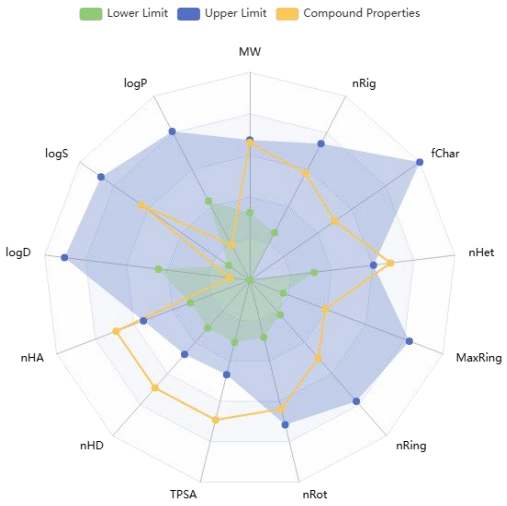

Streptomycin

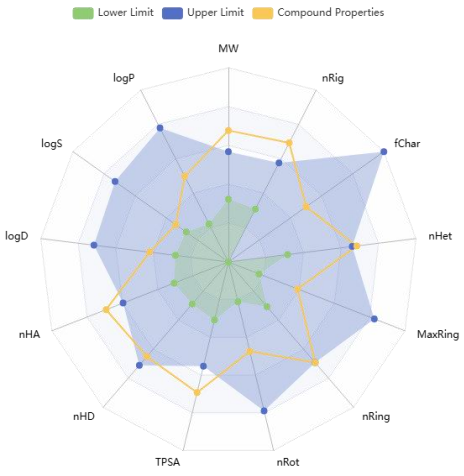

Rifampicin

Figure 4: Radial plot of ADME physicochemical properties of hit compounds

ISSN 0795 - 22066

Principal component analysis

The Principal Component Analysis (PCA) results provided insights into how various ADME physicochemical parameters of the hit compounds influenced their binding at the *M. ulcerans* protein targets. By examining the relationships between the determined molecular descriptors, the properties which contributed to strong or weak ligand-protein interactions were determined. The scree plot showed that three major components with eigenvalues >1 were extracted (Figure 5a). However, the biplot in Figure 5b displayed two components, with PC1 explaining 46.01 % of the variance and PC2 explaining 27.23 %, together accounting for 73.24 % of the total variance. The first principal component (PC1) showed a weak relationship between nA, nRB, TPSA, and HBA with the 4QJL protein of *M. ulcerans*. This weak correlation suggested that these parameters do not significantly contribute to the binding affinity at the 4QJL target. The number of atoms (nA) and the number of rotatable bonds (nRB) are related to molecular flexibility, indicating that more flexible molecules do not strongly favor 4QJL binding. Additionally, TPSA and HBA are indicators of polarity and hydrogen bonding capability, implying that hydrophilic or highly hydrogen-bonding ligands may not efficiently bind to 4QJL. The position of 4QJL on the PCA biplot suggested that other factors, such as MW or log P, might be more relevant for binding at 4QJL. Therefore, ligands targeting 4QJL should not rely solely on hydrogen bonding interactions but should focus on optimizing structural or lipophilic properties to improve their binding affinity at this target.

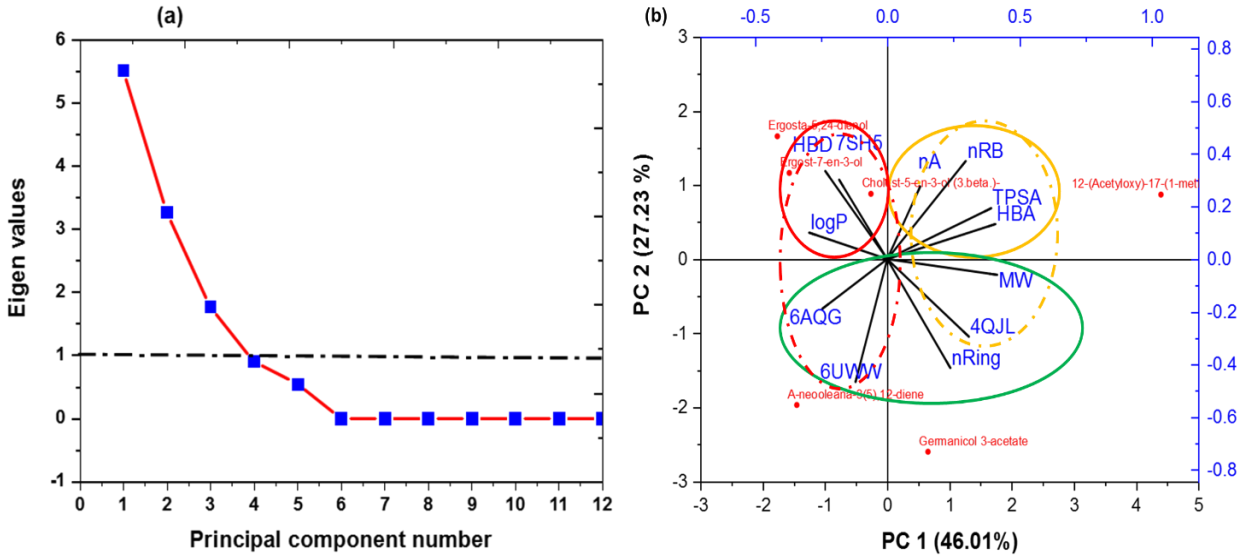

Figure 5: (a) Scree plot and (b) PCA-Biplot of druglikeness properties of the hit compounds and their respective binding energies to the different proteins. Red dots represent the compounds, showing their ADME profiles and binding energies, while broken lines indicate minor relationship

ISSN 0795 - 22066

The second principal component (PC2) indicates a strong relationship between HBD and log P at the 7SH5 target, while also showing weaker relationships with 6AQG and 6UWW. The strong correlation with 7SH5 suggested that ligand binding to this protein is significantly influenced by hydrogen bonding interactions and lipophilicity. HBD play a crucial role in forming hydrogen bonds with active site residues of 7SH5, which may be rich in hydrogen bond acceptors, facilitating stronger interactions [28-29]. Additionally, the log P profile suggested that 7SH5 prefers ligands with moderate hydrophobicity, which may improve both membrane permeability and binding to *M. ulcerans* target. In contrast, the weaker correlations observed with 6AQG and 6UWW indicated that the HBD properties and lipophilicity contribute less significantly to ligand binding at these targets. Therefore, for effective interaction with 7SH5, ligands should be designed with a well-balanced combination of HBD groups and log P. Modifying log P could also enhance bioavailability and protein-ligand interactions, which is critical for effective therapeutic outcomes.

The third principal component (PC3) is associated with a strong relationship between MW and the nRing at the 6UWW, 6AQG, and 4QJL targets. Molecular weight is a key factor for ligand binding, as larger molecules may interact with multiple active site residues, leading to stronger binding affinities. The nRing affects molecular rigidity, and its correlation with 4QJL suggests that rigid, multi-ring structures might be beneficial for binding to this protein. The strong relationship between MW and the 6UWW and 6AQG targets indicates that these *M. ulcerans* proteins may have larger binding pockets that accommodate bulkier ligands, which could be advantageous for the designing of these drugs. Therefore, designing ligands with slightly larger molecular weight and a well-optimized number of rings could enhance their binding affinity at these protein targets. However, excessive molecular weight could impact solubility and metabolic stability, requiring careful optimization to ensure their efficacy.

Generally, the 4QJL target does not strongly favor hydrogen bonding or molecular flexibility, indicating the need for alternative optimization strategies such as increasing rigidity or enhancing hydrophobic interactions to improve binding. The 7SH5 protein strongly correlates with HBD and log P, suggesting that hydrogen bonding and lipophilicity are crucial for effective binding, making these properties key parameters for ligand optimization against *M. ulcerans*. The 6UWW and 6AQG proteins prefer ligands with larger molecular weight and more ring systems, meaning that bulkier and rigid molecules may enhance interactions with these targets, potentially improving therapeutic outcomes.

To rationally optimize ligand design for selective inhibition of *M. ulcerans* protein targets implicated in Buruli ulcer pathogenesis, tailored structural modification strategies should be adopted for each protein. For 4QJL, enhancing

ISSN 0795 - 22066

ligand rigidity or incorporating moieties capable of forming non-classical (non-hydrogen bonding) interactions such as π-π stacking, van der Waals contacts, or halogen bonds may strengthen molecular complementarity and binding affinity. In the case of 7SH5, optimizing the number and positioning of hydrogen bond donors and fine-tuning lipophilicity could improve both binding specificity and pharmacokinetic properties, considering the enzyme's hydrophobic active site environment. For 6UWW and 6AQG, structural optimization efforts should prioritize appropriate adjustment of molecular size and ring systems to enhance steric compatibility with the enzyme active sites and maximize interaction surface area. Collectively, these strategies provide a foundation for the rational design of high-affinity, selective inhibitors with improved drug-like properties for the treatment of Buruli ulcer.

In silico antibacterial activity modeling

Quantitative structure-activity relationship analysis is a crucial computational tool in drug discovery that explores the relationship between the structural characteristics of small molecules and their biological activities [30]. In this study, the AutoQSAR module within the Schrodinger suite was employed, utilizing various topological descriptors to construct independent variable models based on experimental data generated for the target. To evaluate the predictive power of the model, its ability to predict accurately the biological activity of the compounds was tested. The inhibitory activity of two compounds included in the study was calculated using this model. As shown in Figure 6, the linear regression plot comparing predicted versus observed antibacterial activities demonstrates a strong correlation. Furthermore, the statistical performance of the model is summarized in Table 5. The training set yielded a coefficient of determination (R^2) of 0.9124, indicating that approximately 91 % of the variance in biological activity could be explained by the model. This high R^2 value suggested an excellent model fit and highlights the reliability of the AutoQSAR model in accurately predicting the inhibitory potential of structurally related compounds against *M. ulcerans*.

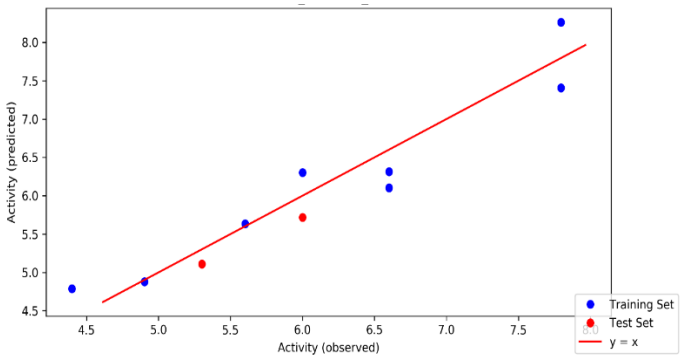

Figure 6: Scatter plot for the best Auto QSAR model

ISSN 0795 - 22066

The root mean square error (RMSE) had a value of 0.2403, showing low prediction error, and the standard deviation (SD) gave a value of 0.3961, reflecting minimal variation in predicted values. For external validation, the model was tested on an independent test set, yielding a cross-validation value (Q^2) of 0.5271, indicating a reasonably good predictive model. These metrics collectively confirmed that the model was statistically robust and capable of reliably predicting the antimicrobial activity of the hit compounds.

Table 5: Parameters for QSAR model

Training Set		Test Set	
SD	R^2	*RMSE*	Q^2
0.3961	0.9124	0.2403	0.5271

The pMIC values obtained from the model were used to determine the minimum inhibitory concentration (MIC) (g/mL) of the studied hit compounds using the relationship:

$$\text{pMIC} = -log_{10}(\text{MIC})$$

The values were then converted to µg/mL unit. This transformation allowed for a more linear comparison of antimicrobial potency across study compounds.

Table 6: Predicted MIC values of hit compounds

Compound	Pred Y (pMIC)	MIC (µg/mL)
Rifampin (WHO)	8.262	0.00548
Clarithromycin (WHO)	6.316	0.48
AMPA	5.921	1.20
Cholest-5-en-3-ol (3.beta.)-	5.887	1.30
Germanicol 3-acetate	5.685	2.07
Ergosta-5,24-dienol	5.638	2.30
A-Neooleana-3(5),12-diene	5.638	2.30
Ergost-7-en-3-ol	5.477	3.34

ISSN 0795 - 22066

In vivo studies have demonstrated that steroidal alkaloids isolated from the aerial parts of *Holarrhena floribunda*, specifically 3-methylamino pregn-5,16-dien-20-ol, 3-methylamino pregn-5-en-20-ol, 3-dimethylamino pregn-5,16-dien-20-ol, and 3-amino pregn-5-en-20-one exhibited significant antimycobacterial activity against *M. ulcerans* [27]. Among these, the fraction containing pure 3-methylamino pregn-5,16-dien-20-ol showed the highest potency, with a minimum inhibitory concentration (MIC) of 50 µg/mL, surpassing the activity of both the other isolated compounds and the crude hydroethanolic extract (MIC = 125 µg/mL), though still less potent than the standard antibiotic Rifampicin (MIC = 2 µg/mL).

In the present study, modeled MIC values for selected hit compounds and reference antibiotics against key *M. ulcerans* targets were determined and are presented in Table 6. The predicted MICs for the hit compounds ranged from 1.20 – 3.34 µg/mL. Notably, AMPA exhibited the highest predicted potency, with an MIC of 1.20 µg/mL, closely followed by cholest-5-en-3-ol (3β)- at 1.30 µg/mL. While these values are higher than those of Rifampicin (0.00548 µg/mL) and Clarithromycin (0.48 µg/mL), the activity of AMPA and cholest-5-en-3-ol (3β)- remains noteworthy and suggests strong potential for further optimization. These findings align with earlier in vivo reports, reinforcing the potential of steroidal scaffolds in the development of novel antimycobacterial agents. Among the compounds evaluated, AMPA emerged as the most promising candidate, exhibiting the lowest MIC and indicating potent inhibitory activity against *M. ulcerans*. The favorable MIC profile of these phytochemicals warrants further investigation through in vitro validation and structure-based optimization to enhance their therapeutic efficacy.

CONCLUSION

This study demonstrates the transformative potential of *in silico* methodologies in accelerating drug discovery for neglected tropical diseases like Buruli ulcer. By integrating gas chromatography-mass spectrometry (GC-MS), molecular docking, ADME profiling, unsupervised machine learning, and AutoQSAR modeling, we identified promising phytochemical inhibitors from tropical medicinal plants, particularly AMPA from *Phyllanthus amarus* and ergosta-5,24-dienol from *Ageratum conyzoides*, with strong binding affinities and favorable pharmacokinetic profiles against essential *Mycobacterium ulcerans* proteins.

Notably, AMPA exhibited potent predicted antibacterial activity with a low MIC value of 1.20 µg/mL, underscoring its potential as a lead compound for future anti-Buruli ulcer therapeutics. Principal Component Analysis revealed that physicochemical descriptors such as lipophilicity, hydrogen bonding, and molecular rigidity significantly influence protein-ligand interactions, offering a rational basis for structure-guided drug optimization.

ISSN 0795 - 22066

Our findings reaffirm the untapped therapeutic reservoir of tropical flora and highlight the capacity of AI-driven screening and modeling to de-risk and streamline early-stage drug development. As global health continues to grapple with antimicrobial resistance and limited access to conventional medicines in endemic regions, this research paves the way for the development of affordable, plant-based, and computationally optimized alternatives for Buruli ulcer management.

Future work should prioritize *in vitro* validation and pharmacodynamic studies to bridge the computational-experimental gap and ultimately translate these bioactive molecules into clinically viable therapeutics. This study serves as a paradigm for intelligent, integrative drug discovery aimed at addressing persistent gaps in global infectious disease control.

FUNDING

This project was sponsored by The Tertiary Education Trust Fund (TETFund) under the TETFund reference number TETF/DR&D/CE/UNI/IMO/IBR/2020/VOL.1

COMPETING INTERESTS

The authors declare no competing interests.

REFERENCES

1. Pearson G. Understanding perceptions on 'Buruli' in northwestern Uganda: a biosocial investigation. *PLoS Negl Trop Dis*. 2018;12(7):e0006689. doi:10.1371/journal.pntd.0006689

2. Zingue D, Bouam A, Tian RBD, Drancourt M. Buruli ulcer, a prototype for ecosystem-related infection, caused by *Mycobacterium ulcerans*. *Clin Microbiol Rev*. 2017;31(1):e00045-17.

3. WHO. Global Buruli Ulcer Initiative. Buruli ulcer (*Mycobacterium ulcerans* infection). Geneva, Switzerland,2018.http://www.who.int/buruli/en/

4. Muleta AJ, Lappan R, Stinear TP, Greening C. Understanding the transmission of *Mycobacterium ulcerans*: a step towards controlling Buruli ulcer. *PLoS Negl Trop Dis*. 2021;15(8):e0009678. doi:10.1371/journal.pntd.0009678

5. Nwofor CN, Duru CE, Onyenwe NE. Retrospective report on the prevalence of Buruli ulcer in Imo State, Nigeria. *Clin Epidemiol Glob Health*. 2024;26:101569. doi:10.1016/j.cegh.2024.101569

6. Hall BS, Hill K, McKenna M, Ogbechi J, High S, Willis AE, Simmonds RE, Taylor MJ. The pathogenic mechanism of the *Mycobacterium ulcerans* virulence factor, mycolactone, depends on blockade of protein translocation into the ER. *PLoS Pathog*. 2014;10(4):e1004061. doi:10.1371/journal.ppat.1004061

7. Beld J, Sonnenschein EC, Vickery CR, Noel JP, Burkart MD. The phosphopantetheinyl transferases: catalysis of a post-translational modification crucial for life. *Nat Prod Rep*. 2014;31(1):61-108.

8. Tamer YT, Gaszek IK, Abdizadeh H, Batur TA, Reynolds KA, Atilgan AR, Toprak E. High-order epistasis in catalytic power of dihydrofolate reductase gives rise to a rugged fitness

ISSN 0795 - 22066

landscape in the presence of trimethoprim selection. *Mol Biol Evol*. 2019;36(7):1533-1550.

9. Terada T, Nureki O, Ishitani R, Ambrogelly A, Ibba M, Söll D, Yokoyama S. Functional convergence of two lysyl-tRNA synthetases with unrelated topologies. *Nat Struct Biol*. 2002;9(4):257-262.

10. Hart BE, Hale LP, Lee S. Recombinant BCG expressing *Mycobacterium ulcerans* Ag85A imparts enhanced protection against experimental Buruli ulcer. *PLoS Negl Trop Dis*. 2015;9(9):e0004046. doi:10.1371/journal.pntd.0004046

11. Boggaram V, Gottipati KR, Wang X, Samten B. Early secreted antigenic target of 6 kDa (ESAT-6) protein of *Mycobacterium tuberculosis* induces interleukin-8 expression in lung epithelial cells via protein kinase signaling and reactive oxygen species. *J Biol Chem*. 2013;288(35):25500-25511.

12. Su CC, Klenotic PA, Cui M, Lyu M, Morgan CE, Yu EW. Structures of the mycobacterial membrane protein MmpL3 reveal its mechanism of lipid transport. *PLoS Biol*. 2021;19(8):e3001370. doi:10.1371/journal.pbio.3001370

13. Campbell EA, Korzheva N, Mustaev A, Murakami K, Nair S, Goldfarb A, Darst SA. Structural mechanism for rifampicin inhibition of bacterial RNA polymerase. *Cell*. 2001;104(6):901-912.

14. Demirci H, Murphy F, Murphy E, Gregory ST, Dahlberg AE, Jogl G. A structural basis for streptomycin-induced misreading of the genetic code. *Nat Commun*. 2013;4:1355. doi:10.1038/ncomms2346

15. WHO. WHO Operational Handbook on Tuberculosis. Module 4: Treatment—Drug-Resistant Tuberculosis Treatment, 2022 update. Web Annexes. 2022. https://iris.who.int/bitstream/handle/10665/365309/9789240065352-eng.pdf

16. O'Brien DP, Friedman ND, Walton A, Hughes A, Athan E. Risk factors associated with antibiotic treatment failure of Buruli ulcer. *Antimicrob Agents Chemother*. 2020;64(9):e00722-20. doi:10.1128/AAC.00722-20

17. Tsouh FPV, Nyarko AK, Appiah-Opong R, Tchokouaha Yamthe LR, Ofosuhene M, Boyom FF. Update on medicinal plants with potency on *Mycobacterium ulcerans*. *Biomed Res Int*. 2015;2015:917086.doi:10.1155/2015/917086

18. Osei-Owusu J, Aidoo OF, Eshun F, Quansah EO, Asiedu-Gyekye IJ, Mensah AY. Buruli ulcer in Africa: geographical distribution, ecology, risk factors, diagnosis, and indigenous plant treatment options- a comprehensive review. *Heliyon*. 2023;9(11):e22018. doi:10.1016/j.heliyon.2023.e22018

19. Andreoli A, Mou F, Minyem JC, Boreux R, Carbonnelle B, Antoine R, Muyembe JJ. Complete healing of a laboratory-confirmed Buruli ulcer lesion after receiving only herbal household remedies. *PLoS Negl Trop Dis*. 2015;9(11):e0004102. doi:10.1371/journal.pntd.0004102

20. Enenebeaku UE, Duru CE, Mgbemena IC, Ukwandu NCD, Nwigwe HC, Enenebeaku CK, Okotcha EN. Phytochemical evaluation and molecular docking of bioactive compounds from the roots of *Dictyandra arborescens* (Welw.) against *Plasmodium berghei* protein targets. *Trop J Nat Prod Res*. 2021;5(2):370-381.

21. Megantara S, Iwo MI, Levita J, Ibrahim S. Determination of ligand position in aspartic proteases by correlating Tanimoto coefficient and binding affinity

ISSN 0795 - 22066

with root mean square deviation. *J Appl PharmSci*.2016;6(1):125-129.

22. Duru CE, Duru IA, Ikpa CBC, Enenebeaku UE, Obiagwu IC, Igbomezie MC, Nnabuchi MA. In silico docking studies of bioactive compounds in *Ocimum gratissimum* essential oil against Candidapepsin-1 enzyme from *Candida albicans*. *Trop J Nat Prod Res*. 2021;5(2):364-369.

23. BIOVIA. Dassault Systemes, San Diego. *Discovery Studio Modeling Environment*. 2020.

24. Duru CE. Forever chemicals could expose the human fetus to xenobiotics by binding to placental enzymes: prescience from molecular docking, DFT, and machine learning. *Comput Toxicol*. 2023;100274.doi:10.1016/j.comtox.2023.100274

25. Coulibaly B, N'guessan KR, Aka N, Koffi KPB, Djaman AJ, Dosso M. In vitro antimycobacterial activity of extracts of *Phyllanthus amarus* (Schum and Thonn) on *Mycobacterium ulcerans* strains in Côte d'Ivoire. *Bull Soc Roy Sci Liege*. 2011;80:759-771.

26. Trebissou JND, Beourou S, Lohoues EEC, Yapi HF, Boga GL, Djaman AJ. In vitro evaluation of the activity of aqueous extract of a plant coded phyllam (phyllanthus amarus) on two strains of *Mycobacterium tuberculosis* and one strain of *Mycobacterium ulcerans*. *World J Pharm Res*. 2013;2(6):1878-1888.

27. Yemoa A, Gbenou J, Affolabi D, Moudachirou M, Quetin-Leclercq J, Van Puyvelde L. Buruli ulcer: a review of in vitro tests to screen natural products for activity against *Mycobacterium ulcerans*.*PlantaMed*2011;77:641-646.

28. Enyoh CE, Wang Q. Automated classification of undegraded and aged polyethylene terephthalate microplastics from ATR-FTIR spectroscopy using machine learning algorithms. *J Polym Environ*. 2024.doi:10.1007/s10924-024-03199-4

29. Enyoh CE, Wang Q. Box–Behnken design and machine learning optimization of PET fluorescent carbon quantum dots for removing fluoxetine and ciprofloxacin with molecular dynamics and docking studies as potential antidepressant and antibiotic. *Sep Purif Technol*. 2025;362(5):131975. doi:10.1016/j.seppur.2025.131975

30. De P, Kar S, Ambure P, Roy K. Prediction reliability of QSAR models: an overview of various validation tools. *Arch Toxicol*. 2022;96(5):1279-1295. doi:10.1007/s00204-022-03252-y

ISSN 0795 - 22066